Petroleum Science 19 (2022) 486–497

Contents lists available at ScienceDirect

Petroleum Science

journal homepage: www.keaipublishing.com/en/journals/petroleum-science

Original Paper

Distribution characteristics and oil mobility thresholds in lacustrine shale reservoir: Insights from N_2 adsorption experiments on samples prior to and following hydrocarbon extraction

Long-Hui Bai [a], Bo Liu [b, a, *], Yi-Jing Du [c], Bo-Yang Wang [a], Shan-Si Tian [a], Liu Wang [a], Zhi-Qiang Xue [d]

[a] Accumulation and Development of Unconventional Oil and Gas, State Key Laboratory Cultivation Base, Northeast Petroleum University, Daqing, Heilongjiang 163318, China
[b] Hubei Key Laboratory of Petroleum Geochemistry and Environment, Yangtze University, Wuhan, Hubei 430100, China
[c] Research Institute of Petroleum Exploration & Development, Beijing, 100083, China
[d] No.1 Institute of Geological and Mineral Resources Survey of Henan, Luoyang, Henan 471000, China

ARTICLE INFO

Article history:
Received 27 February 2021
Accepted 21 June 2021
Available online 23 October 2021

Edited by Jie Hao

Keywords:
Shale oil mobility
Oil phase state
Extraction
Nitrogen adsorption

ABSTRACT

The pore structure and oil content of shales have an important influence on the oil mobility and enrichment. In this study, the lacustrine shale samples from the Qingshankou Formation (Q1) of Songliao Basin were selected. TOC, pyrolysis, XRD and nitrogen adsorption were performed on the original and extracted shale samples. Then the influence of mineral composition and organic matter (OM) on the development of nano-scale pore, the oil phase states and mobility were analyzed. The Q1 shale samples can be sub-divided into three types according to the isotherm characteristics. Type A samples are characterized by high kerogen content, with oil mainly existing in the free phase state. Type B samples are characterized by medium kerogen content, oil mainly exists in the absorbed phase state. Type C samples are characterized by low kerogen content, with trace oil found in the absorbed phase state. Nano-scale organic pores are well developed in the Q1 Formation. Oil is primarily found in the pore spaces with diameters less than 10 nm, this being the pore size threshold for mobile shale oil. When TOC_o > 2.0 wt% and EOM >1.0 wt%, Q1 Formation shale oil mobility is high, resulting in prospective drilling targets.

1. Introduction

More and more attention was being paid to the exploration and development on shale oil and gas reserves, this due to the gradual depletion of conventional oil and gas reserves and the increasing difficulty in the exploration and development of new conventional reserves. In recent years, shales have been widely studied as oil and gas reservoirs. Recently, the successful development of shale oil and gas resources in North America has even changed the pattern of the world energy supply (Zou et al., 2015; Curiale and Curtis, 2016). China has also gradually increased the exploration and development of shale oil and gas resources (Zou et al., 2015; Hu et al., 2017; Liu et al., 2019a). The main difference between shale reservoirs and conventional reservoirs, is that shale is also the source rock for oil generation as well as the reservoir, with low porosity and permeability typically encountered (Ross and Bustin, 2007; Ghanizadeh et al., 2014; Gong et al., 2021). This means that for shale reservoirs, the following factors strongly influence the understanding of shale storage capacity and charge mechanisms: pore structure development, the distribution characteristics of mobile oils, and the percentage of shale oil in different phase states have an important influence on the understanding of shale storage capacity and enrichment mechanism (Xie et al., 2019; Liu et al. 2019a, 2021a).

In shale reservoirs, various pore types can develop. These include interparticle pores, intraparticle pores, organic matter (OM) pores and microfractures. All these pore types are observed on a nano-scale usually (Loucks et al., 2012). The development of pore space is primarily controlled by mineral composition, depositional sedimentary environment, OM characteristics and tectonic

* Corresponding author. Hubei Key Laboratory of Petroleum Geochemistry and Environment, Yangtze University, Wuhan, 430100, China.
E-mail address: liubo@nepu.edu.cn (B. Liu).

https://doi.org/10.1016/j.petsci.2021.10.018

developed history of the reservoir (Loucks et al., 2012; Gao and Hu, 2018; Dong et al., 2019; Gao et al., 2020). In contrast to conventional reservoirs, OM is one of the important components of shale, and its content, type and maturity have a major impact on the development of pore space in shale (Pepper and Corvi, 1995; Pitman et al., 2001; Curtis et al., 2012; Huang et al., 2013; Dong et al., 2019). OM in shales can be sub-divided into insoluble OM (kerogen), soluble hydrocarbon, polar organic compounds and other components, according to whether it can be dissolved in organic solvents (Littke et al., 1991). The fractional content of soluble OM can generally be used to evaluate the fractional content of oil in shale reservoirs.

The pore space of the shale reservoirs comprises the main storage space for the hydrocarbons generated from mature OM. Significantly different from the shale gas reservoir, when the OM is in the main oil generation window; in shale oil reservoirs, the effect of the generated hydrocarbons occupying pore space will inevitably have an impact on the measurement results. Yet, the related research is rare, and the quantitative research on the distribution of shale oil in the pore space of different pore sizes is also lacking (Xie et al., 2019). Additionally, during the quantitative evaluation of pore space characteristics, determining parameters such as porosity, pore size distribution and the OM characteristics will inevitably have a certain impact on the measurement results, but there are few related studies. More research is required to fully understand the role of hydrocarbons on petrophysical properties within the oil window (Xie et al., 2019). Quantitative studies on the distribution of mobile oil in nano-scale pore spaces are also required. At present, fluid injection methods, including mercury injection and nitrogen adsorption are the quantitative analysis tools used to determine shale porosity and pore size distribution mainly uses the fluid injection method including mercury injection and nitrogen adsorption (Gao and Hu, 2016; Liu et al. 2018, 2021b; Dong et al., 2019; Xie et al., 2019; Zeng et al., 2021).

In this study, the lacustrine, organic-rich shale samples from the first member of Qingshankou (Q1) Formation in Songliao Basin were targeted, and the shale samples with different OM content that were in the main oil generation window were selected. Chloroform was used as organic solvent to extract the soluble OM from the shale samples, to quantify the mobile oil in the Q1 shale reservoir. Mineral composition, TOC, pyrolysis and nitrogen adsorption experiments were carried out on the samples prior to and following hydrocarbon extraction to study the influence of shale composition on the development of pore space, and the relationships between pore size and the distribution of mobile shale oil in nano-scale pore spaces. Finally, the thresholds of mobile shale oil in the Q1 Formation were determined.

2. Samples and methods

The Songliao Basin is a world continental petroliferous basin located in Northeast China. The thickest and most widely distributed interval in the basin is of Cretaceous age (Liu et al., 2017). The Q1 Formation formed during the initial growth of the basin, which belongs to the deep and semi deep lake sedimentary environment. The climate was warm and humid, and the aquatic organisms were flourishing. A sequence of dark, organic-rich shales with a thickness around 100 m was deposited. The abundant OM is mainly composed of mature, oil-prone Type I and Type II kerogen, which has excellent hydrocarbon generation potential (Liu et al. 2019b, 2021a).

In this study, samples were taken from the Cretaceous Q1 Formation in the Qijia and Gulong sag. 10 lacustrine, organic rich dark shale samples with similar maturity (in the oil generation window) and with TOC_0 ranging from 0.4 wt% to 4.0 wt% were selected.

First, each sample was divided evenly into two parts. One part was used to determine the mineral and OM composition and the pore size distribution of the original shale samples using nitrogen adsorption. The mineral composition was determined using a D8AA25 X-ray diffractometer. A CS 230 carbon sulfur analyzer and a Rock Eval 6 were used to identify the shale OM characteristics, including TOC and hydrocarbon generation potential characteristics. The process used to determine shale mineralogy and OM composition followed the procedure described by Liu (Liu et al., 2019b). Along with quartz, feldspar, clay and carbonate mineral content, and the OM parameters derived include TOC, S_1, S_2, S_3, T_{max} and HI (HI $= S_2/\text{TOC} \times 100$) are obtained. The remaining original samples were crushed to 60–80 mesh and dried at 105 °C to obtain the pore volume and pore size distribution using nitrogen adsorption. Hydrocarbon extraction was performed on a third part of the sample via Soxhlet extraction using chloroform as the solvent. The extraction was performed at 70 °C for a period of 48 h to allow quantification of mobile oil in the shale samples. Following the extraction experiment, the shale sample particles without mobile oil were recovered and dried at 105 °C. Subsequently, these samples that had undergone extraction were subjected to TOC, pyrolysis and nitrogen adsorption experiments once more.

Many theoretical methods could be used to interpret the nitrogen adsorption result in order to obtain pore size distribution information, such as Brunauer-Emmett-Teller (BET), Barrett-Joyner-Halenda (BJH) and Density-Functional-Theory (DFT). However not all theoretical methods are suitable for characterizing the pore structure of shale, some are limited by the assumptions inherent in the method, or by the complex composition and pore structure of shale, not all theoretical methods are suitable for characterizing pore structure of shale (Barrett et al., 2014; Villarroel-Rocha et al., 2014; Zhang et al., 2017; Liu and Ostadhassan., 2019). Considering the applicability of each theoretical method, we chose to use the BET model to obtain the shale specific surface area (SSA), the BJH model to obtain pore volume and average pore size and the DFT model to obtain pore size distribution characteristics.

3. Results

3.1. Composition of the Q1 shale sample

3.1.1. XRD

The XRD results show that the selected shale samples are primarily composed of clay, quartz and feldspar (Fig. 1). The content of

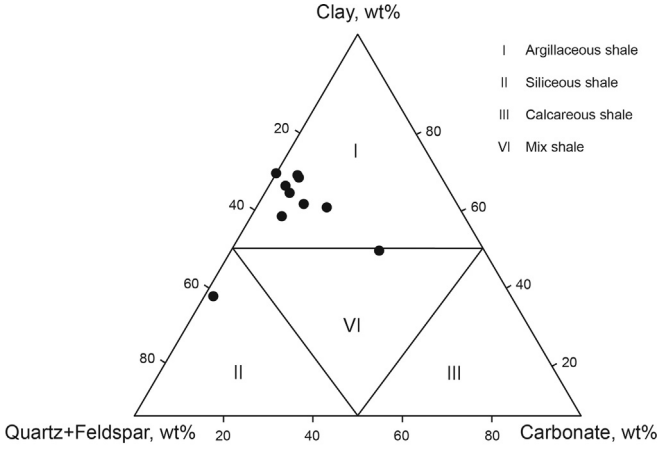

Fig. 1. (a) Triangular plot of rock mineral composition of the selected shale samples from the Q1 Formation (modified and simplified from Gamero-Diaz et al., 2013).

clay ranges from 32.2 wt% to 64.0 wt%, with an average content of 54.9 wt%, and the clay content of all samples is more than 50 wt% mostly. The content of quartz ranges from 18.7 wt% to 53.6 wt%, with an average content of 28.69 wt%. The feldspar is mainly composed of plagioclase, with an average content of 7.65 wt%, and the content ranges from 4.5 wt% to 12.8 wt%. The content of carbonate ranges from 0 wt% to 33.5 wt%, with an average content of 8.86 wt%, of which are mainly composed of calcite and a small amount of ankerite. It should be noted that the content of carbonate in I2-3 sample is the highest, with the calcite content of 33.5 wt%, while the carbonate content of other samples is basically lower than 15.0 wt%. Pyrite is ubiquitous in all samples, with an average content of 1.64 wt%. According to the mineral composition diagram, the shale samples are mainly argillaceous shale, followed by siliceous shale and mixed shale (Fig. 1).

3.1.2. OM composition characteristic of original and extracted shale sample

For the original shale samples selected in this study, the content of TOC_o ranges from 0.49 wt% to 4.08 wt%, with an average content of 2.20 wt%. The content of free hydrocarbon S_1 ranges from 0.75 mg/g to 6.22 mg/g, with an average content of 3.73 mg/g. The content of pyrolysis hydrocarbon S_2 ranges from 1.18 mg/g to 14.32 mg/g, with an average content of 8.32 mg/g. The values of hydrocarbon index HI range from 241 mg/g to 470 mg/g, with an average value of 372 mg/g. After extraction, the content of TOC_e ranges from 0.33 to 3.01 wt%, with an average content of 1.55 wt%. The content of free hydrocarbon S_1 ranges from 0.04 mg/g to 0.40 mg/g, with an average content of 0.22 mg/g. The content of pyrolysis hydrocarbon S_2 ranges from 0.36 mg/g to 5.25 mg/g, with an average content of 2.35 mg/g. The values of hydrocarbon index HI range from 64 mg/g to 200 mg/g, with an average value of 136 mg/g (Table 1).

By comparing the geochemical results of original and extracted shale samples from the Q1 Formation, it can be seen that the contents of the TOC_e, S_1, S_2 and S_3 of the extracted samples all decrease to differing degrees (Fig. 2a–d). The content of S_1 decreases the most after extraction, indicating that S_1 is mainly composed of soluble OM (Jarvie et al., 2007). Meanwhile, the contents of S_2 and S_3 also decrease, which indicates that the content of soluble OM also contributes to the contents of S_2 and S_3. Furthermore, it should be noted that the abnormal increase in S_2 and TOC values from individual samples following extraction was observed, this may be due to the sample heterogeneity. Additionally, the content TOC of the extracted shale samples mainly represents the content of the kerogen (Fig. 2d), which in turn indicates that the insoluble solid OM (kerogen) is the largest contributor to the total OM quantity.

The T_{max} value of the extracted shale samples generally increases, which is due to the decrease in light hydrocarbon content after extraction. Relatively light hydrocarbons and non-hydrocarbons are included in the S_2 measurement, which will result in a drop in the peak temperature of S_2 drop (Collins and Lapierre., 2014; Carvajal-Ortiz and Gentzis., 2015). Correspondingly, the original shale samples contain mainly Type IIA kerogen (Fig. 3a) according to the plot of T_{max} versus HI (Espitalié et al., 1984). After extraction, while a small reduction of TOC was noted, the value of the HI index reduced significantly due to the loss of light hydrocarbons belonging to S_2 during the extraction process. This indicates that the extracted shale samples are mainly composed of Type IIB and Type III kerogens according to the plot of T_{max} versus HI. The derived TOC content from the extracted shale samples is strongly influenced by kerogen content. These TOC values show a good linear correlation with S_1 and extractable OM (EOM), with the coefficients of $R^2 = 0.69$ and $R^2 = 0.71$, respectively. In addition, the total oil (total oil = $(S_1+S_2)_{original}$ - $(S_1+S_2)_{extracted}$) (Jarvie, 2012) obtained from pyrolysis parameters before and after extraction show a good correlation with TOC_e (Fig. 3b and c). This indicates that kerogen is the primary oil generation material. Under the similar geological conditions, the kerogen content is the main factor determining the eventual oil content. It also shows that the total oil, EOM and S_1 all can indicate the relative content of mobile shale oil.

It should be noted that the values obtained for S_1 in this study are generally 2 times higher than the values published by Liu et al (Liu et al. 2019a, 2019b). That is because these samples were investigated almost as soon as they were extracted from the well. EOM values however, show a similar distribution range when compared to the results of earlier studies, indicating that EOM is a better parameter to consider S_1 when characterizing the content of soluble OM (i.e. shale oil) (Behar et al., 2001; Liu et al., 2019b).

3.2. Nitrogen adsorption of the original and extracted shale samples

3.2.1. Adsorption isotherms

Typical nitrogen isotherms of this study are shown in Fig. 4. According to the characteristics of nitrogen isotherms of shale samples before and after extraction, it can be divided into three groups. The samples with Type A isotherms include I1-1, I1-2, I1-5 and I2-3, these correspond to isotherm of type II defined by IUPAC (Sing, 1985; Sing et al., 2016). The hysteresis loops are small, and the isotherms increase to infinity when $p/p_o = 1$, this indicating the existence of macropores. Furthermore, the hysteresis loops of Type A isotherms are similar to that of type H3, indicating the pores are composed of parallel plate pores. The hysteresis loop changed considerably after extraction, and came to resemble type H2B. This indicates the pores are ink bottle pores, which is clearly a different result from the original shale samples. The amount of nitrogen

Table 1
Bulk geochemical parameters and XRD results of the selected shale samples from the Q1 Formation.

Number	Rock-Eval (Original)					Rock-Eval (Extracted)					Whole Rock Mineralogy (wt.%)						EOM (wt.%)
	TOC (wt.%)	T_{max} (°C)	S_1 (mg HC/g)	S_2 (mg HC/g)	S_3 (mg HC/g)	TOC (wt.%)	T_{max} (°C)	S_1 (mg HC/g)	S_2 (mg HC/g)	S_3 (mg HC/g)	Quartz	Plagioclase	Calcite	Ankerite	Pyrite	Total Clay	
I1-1	3.25	437	6.22	13.00	1.60	2.46	452	0.34	3.89	0.36	28.3	7.7	0	0	0	64.0	1.35
I1-2	2.85	428	5.02	11.20	1.35	1.89	454	0.26	3.78	0.34	25.7	9.7	2.0	0	1.9	60.6	1.49
I1-3	0.49	405	0.75	1.18	0.16	0.56	440	0.07	0.46	0.04	29.8	10.6	3.5	0	3.5	52.6	0.75
I1-4	2.13	421	3.85	8.45	1.02	1.32	445	0.19	1.43	0.13	25.8	6.0	3.9	0	1.8	63.1	3.33
I1-5	2.59	452	2.75	8.00	0.89	1.87	441	0.20	2.13	0.19	20.9	8.2	9.0	3.7	3.2	54.9	1.02
I2-1	1.97	420	3.44	5.91	0.78	0.93	422	0.10	0.59	0.06	53.6	12.8	0	0	1.5	32.2	1.26
I2-2	1.94	420	4.11	8.65	1.07	1.37	445	0.22	2.08	0.19	28.4	5.6	5.6	3.7	0.9	55.8	1.13
I2-3	4.08	453	5.29	14.32	1.63	3.01	445	0.35	5.25	0.46	18.7	4.5	33.5	0	0	43.3	0.16
I2-4	2.17	435	4.06	10.19	1.18	1.78	446	0.40	3.53	0.33	26.2	5.2	3.5	0	1.7	63.4	0.51
I2-5	0.56	426	1.78	2.28	0.34	0.33	435	0.04	0.36	0.03	29.5	6.2	3.8	0	1.9	59.1	0.72

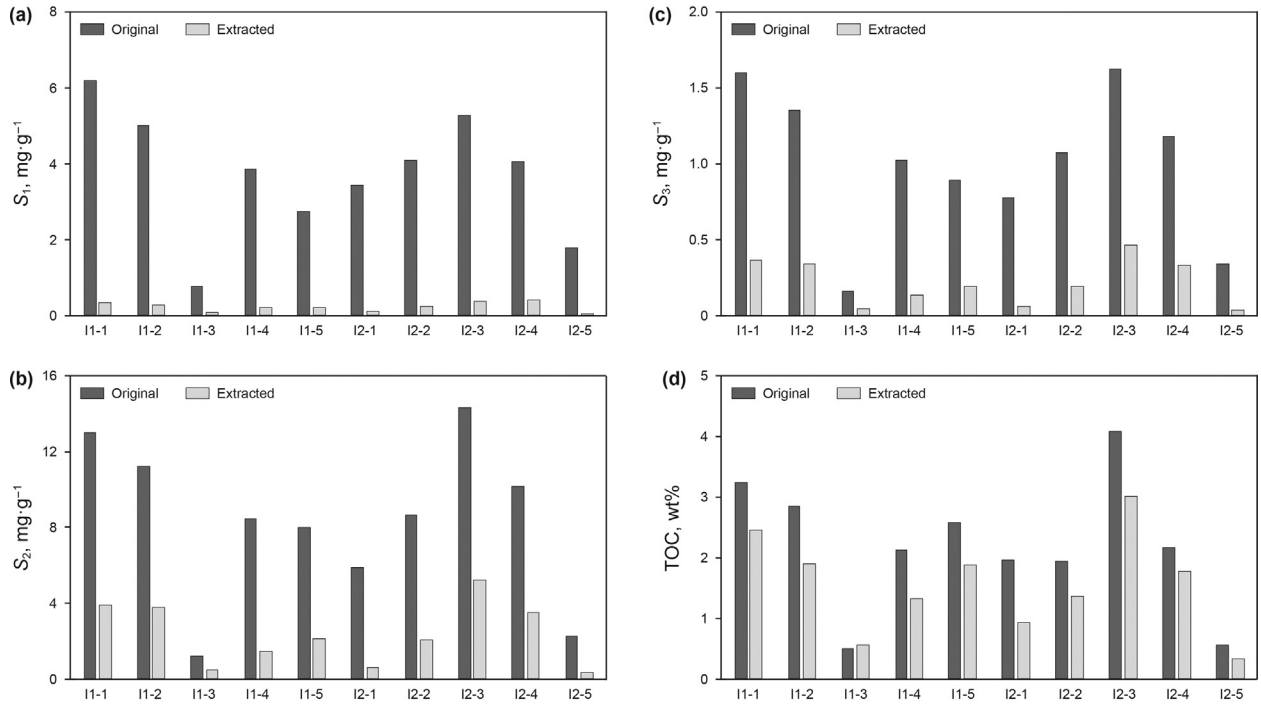

Fig. 2. Bar chart of comparing bulk geochemical results between original and extracted shale samples (a) free hydrocarbon S_1. (b) pyrolysis hydrocarbon S_2. (c) organic carbon S_3. (d) Total organic carbon TOC.

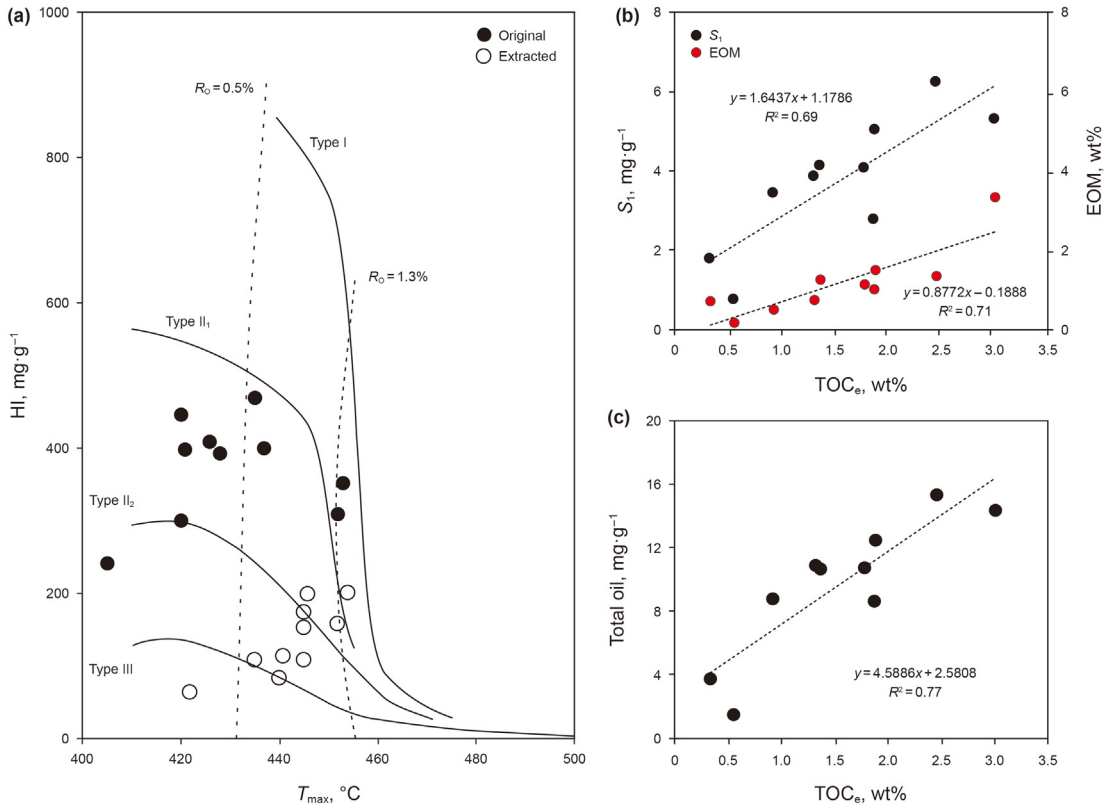

Fig. 3. Crossplots of the bulk geochemical results. (a) Hydrogen index (HI) versus T_{max} relationship for the original and extracted shale samples from the Q1 Formation. (b) Crossplots of TOC versus S_1 and EOM. (c) Crossplots of TOC versus total oil.

adsorbed increases obviously under the same relative pressure after extraction (Fig. 4a). The samples with Type B isotherms include I1-7, I2-2 and I2-4. The isotherms before and after extraction both correspond to isotherms of type VI, the hysteresis loops before and

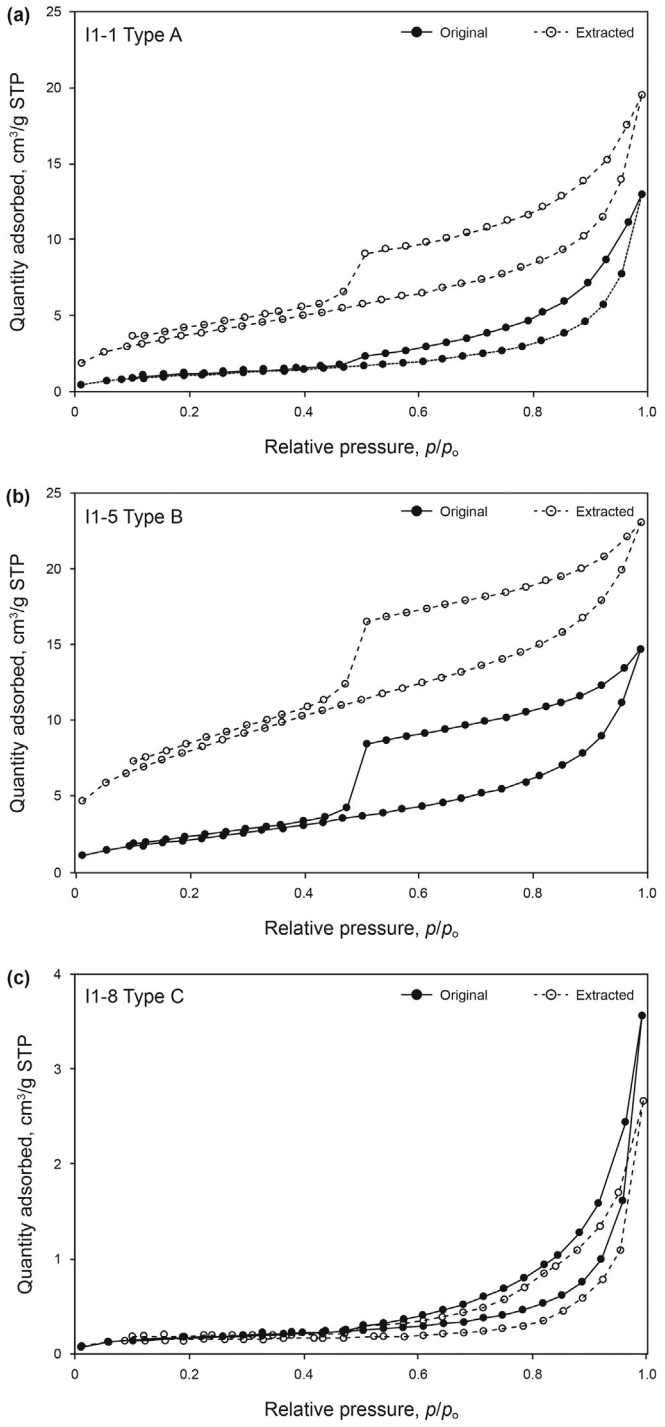

Fig. 4. Typical nitrogen isotherms of the original and extracted shale samples for the Q1 Formation.

after extraction are both similar to type H2B, which indicates that the pores are composed of ink bottle pores. Similar to the Type A samples, the nitrogen adsorption capacity of the extracted shale increased significantly under the same relative pressure compared with that of the original samples (Fig. 4b). The samples with Type C isotherms include I1-4, I2-1 and I2-5. Similar to Type B, the derived isotherms from this subset correspond to type II isotherms, and the hysteresis loops measured before and after extraction are both similar to type H3. That indicates that the pores of original and extracted samples are both composed of parallel plate pores. By contrast to Type A and B samples, the Type C shale samples have almost the same amount of nitrogen adsorption capacity under the same pressure regime. The gas adsorption amount capacity of Type C shale samples in the same relative pressure range is significantly lower than that of Type A and B shale samples (Fig. 4c).

3.2.2. Specific surface area

For the original shale samples, the BET results show that the specific surface area ranges from 0.1245 m^2/g to 4.8975 m^2/g, with an average specific surface area of 2.816 m^2/g. After extraction, the specific surface area of shale samples increased significantly. The specific surface area ranges from 0.3522 m^2/g to 13.7433 m^2/g, with an average specific surface area of 6.6495 m^2/g (Table 2).

3.2.3. Pore volume and average pore diameter

For the original shale samples, the BJH results indicate that the pore volume ranges from 0.001178 cm^3/g to 0.020215 cm^3/g, with an average pore volume of 0.0144577 cm^3/g. The average pore diameter ranges from 12.655 nm to 37.2128 nm. After extraction, the pore volume ranges from 0.001614 cm^3/g to 0.03003 cm^3/g, with an average pore volume of 0.0182086 cm^3/g. The average pore diameter ranges from 8.6922 nm to 23.0636 nm (Table 2).

The average pore diameter of the shale samples after extraction is smaller than that of the original samples (Fig. 5a), while the pore volume of the shale samples after extraction is typically larger than that of the original shale samples (Fig. 5b). Yet, the pore volume of the I1-3 and I2-1 samples after extraction is smaller than that of the original shale samples, and the pore volume of the I2-5 samples is nearly the same as the original sample after extraction. Average pore diameter exhibits a good negative correlation with pore volume of the original and extracted shale samples, indicating that the nano scale micropore development provides a lot of pore space in the Q1 shales (Fig. 5c and d).

3.2.4. Pore size distribution

Most of the original shale samples have bimodal pore size distribution with peaks at 10 nm and 40 nm. The pores of I1-3, I1-4, I2-1 and I2-5 show a large percentage of pores with diameter of around 40 nm, which basically belong to Type C shale samples. However, the total pore volume of these samples is not developed. The range of longitudinal pore volume is obviously lower than that of other samples (Fig. 6).

The pore volumes of samples I1-3, I1-4, I2-1, I2-3 and I2-5 after extraction have no obvious variations with pore size distribution, and the pore volumes of I1-3 and I2-1 shale samples with Type C isotherm are even lower than those of the original samples. In these samples, the pore volume of diameter less than 10 nm is high compared to that of other samples after extraction. However, the pore volume does not vary significantly in the range of pore diameter greater than 10 nm after extraction (Fig. 6).

4. Discussion

4.1. Influence of shale composition on nano-scale pore development in the Q1 shales

The Type A shale samples have the largest EOM content (0.75–3.33 wt%), followed by the Type B shale samples (1.02–1.26 wt%), and that of Type C shale samples have the lowest EOM content (0.16–0.72 wt%) (Fig. 7a). The content of free oil is controlled by the amount of kerogen. After extraction, the TOC_e of Type A shale samples is the highest (TOC_e ranges from 1.32 wt% to 3.01 wt%), followed by Type B shale samples (TOC_e ranges from 1.37 wt% to 1.87 wt%), and the lowest is found in Type C shale

Table 2
BET surface area, pore volume and average pore size results of the raw and extracted shale samples from Q1 Formation.

Number	Isotherm type	Original			Extracted		
		surfacea rea (m^2/g)	Pore volume (cm^3/g)	Average pore size (nm)	surfacea rea (m^2/g)	Pore volume (cm^3/g)	Average pore size (nm)
I1-1	A	3.9132	0.020068	18.3009	13.7433	0.03003	8.6922
I1-2	A	2.8853	0.015015	18.7172	9.604	0.022993	9.3906
I1-3	C	0.6301	0.005513	31.5618	0.486	0.001614	17.3255
I1-4	A	2.0207	0.011959	21.3967	4.4168	0.015904	13.4775
I1-5	B	3.2374	0.016204	17.5626	6.7611	0.017577	10.2448
I2-1	C	4.8975	0.01918	12.655	6.2547	0.017282	10.657
I2-2	B	3.3956	0.017108	17.172	10.4009	0.025403	8.9979
I2-3	A	2.5164	0.018137	26.0592	5.2673	0.02252	16.2259
I2-4	B	4.5355	0.020215	15.0404	9.2087	0.02673	10.4058
I2-5	C	0.1245	0.001178	37.2128	0.3522	0.002033	23.0636

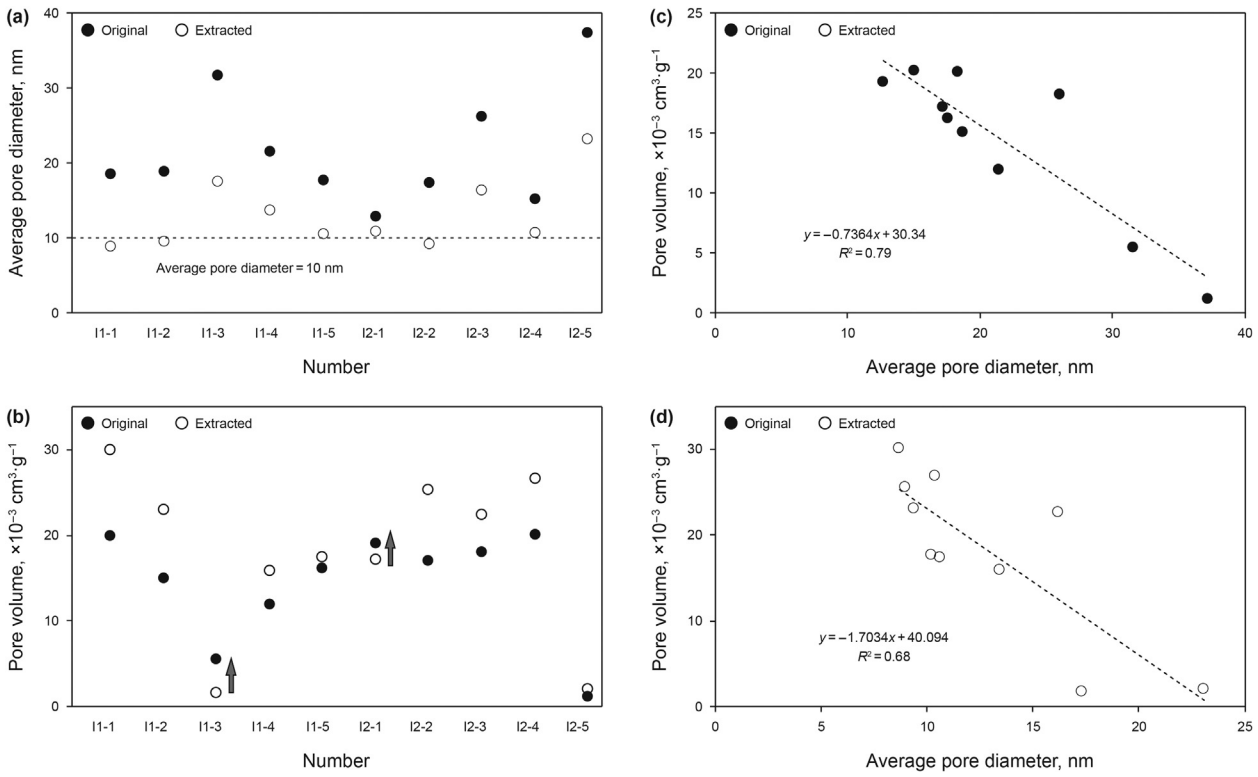

Fig. 5. Distributions (a, b) and Crossplots (c, d) of the nitrogen adsorption experiment results. (a) The average diameter of the original and extracted shale samples. (b) The pore volume of the original and extracted shale samples. (c) The pore volume versus the average diameter of the original shale samples. (d) The pore volume versus the average diameter of the extracted shale samples.

samples (TOC_e ranges from 0.33 wt% to 0.92 wt%). Hence, the kerogen content of Type A shale samples is the highest, EOM is the highest, followed by Type B shale samples, with Type C shale samples having the lowest content of kerogen and EOM (Fig. 7b). Pores smaller than 40 nm were mainly developed in the Type A and B shale samples before extraction, and pores less than 10 nm have significantly developed after extraction predominated (Fig. 6). The Type A and B shale samples are significantly properties to Type C shale samples. In Type C shale samples, measured EOM is 1.0 wt%, and the TOC_o and TOC_e are 2.0 wt% and 1.4 wt%, respectively.

Type A and B shale samples have relatively low quartz and feldspar contents, and relatively high clay and carbonate contents (Fig. 7c–e). Type C shale samples are rich in rigid minerals such as quartz and feldspar (Fig. 7 c). The pore space of Type C shale samples prior to and after extraction is poorly developed, and the pore volume is relatively low. It can be clearly seen that pores with a pore diameter of around 40 nm are developed. This is because rigid minerals such as quartz and feldspar play a role in protecting relatively large primary pore space during burial and compaction (Loucks et al., 2012; Dong et al., 2019). Clay minerals, due to their large specific surface area, provide space for OM (Kennedy et al., 2014; Su et al., 2018; Liu et al. 2020), and can also form a “card house” micro pore structure (Bennett et al. 1991; Slatt and O’Brien, 2011)). Kerogen also has a large specific surface area, which again is also conducive to the development of nano scale reservoir space (Dong et al., 2018; Slatt and O’Brien, 2011). The chemical instability of carbonate minerals means that they are easily affected by organic acids produced during hydrocarbon generation, which again is favorable for the development of micropores. Type A and B shale samples are rich in clay, OM and carbonate minerals (Fig. 7a–e), which not only leads to the generation of pores with a maximum diameter of around 40 nm, but also is favorable for the

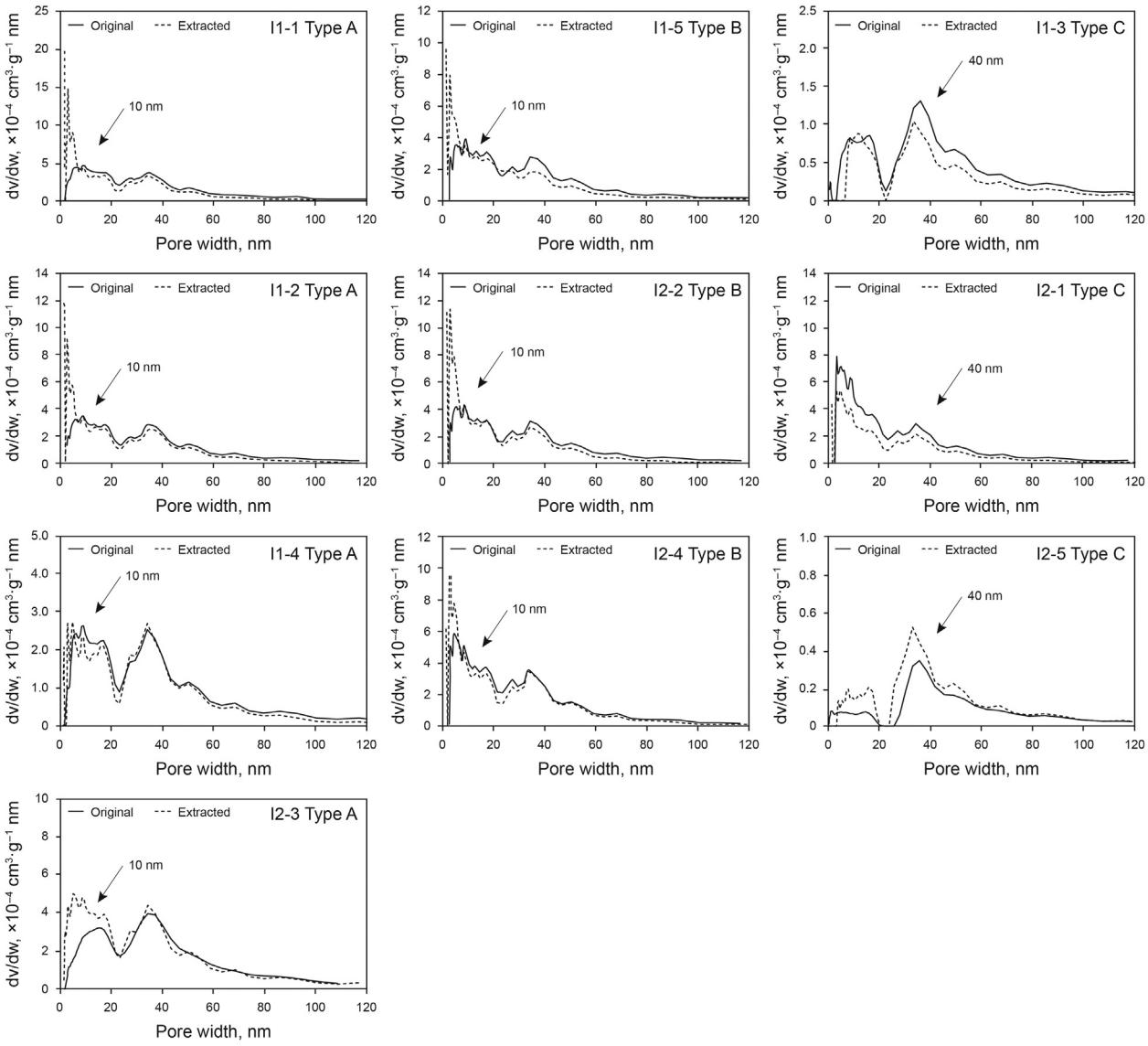

Fig. 6. The pore size distributions of the original and extracted shale samples for the Q1 Formation.

development of pore space with a pore diameter around 10 nm (Fig. 6). After extraction, the total pore volume of Type A and B shale samples also increased significantly, while that of Type C shale samples remained almost unchanged (Fig. 7f).

4.2. Effect of soluble OM on nitrogen isotherm

Examination of nitrogen isotherms from shale samples before and after extraction show that the content of soluble OM has a significant impact on gas adsorption and desorption behavior (Figs. 4 and 7). In Type A shale samples, kerogen is well developed. Plenty of mobile shale oil is available to fill in the pore space, resulting in the variation of original characteristics of pores. After extraction, the recorded hysteresis loops of the unmodified sample change from type H3 indicating plate parallel pores, to type H2B typical of small-diameter ink bottle pores. The nitrogen adsorption capacity increased significantly due to volume of pore space made available following oil removed during extraction. In Type B shale samples, the content of kerogen and shale oil in the pore space is relatively high. However, the shale oil in Type B shale samples is mainly in the absorbed phase state, and the content of adsorbed shale oil is not enough to change the original pore space characteristics. Hence, the hysteresis loops of both original and extracted samples are mainly of type H2B, indicating the presence of ink bottle pores. The removal of adsorbed shale oil after extraction would also release a large amount of specific surface, resulting in a significant increase in the nitrogen adsorption capacity. In Type C shale samples, the content of kerogen and shale oil are relatively low. The shale oil mainly exists in the adsorbed phase state, which is similar to that of Type B shale sample. The trace amounts of adsorbed shale oil in Type C shale samples are also not enough to change the original pore characteristics during oil charge (Fig. 8). Therefore, the nitrogen isotherms from Type C samples prior to and after extraction are all H3 hysteresis loops, indicating plate parallel pores. Furthermore, the nitrogen adsorption capacity of these samples is almost identical from samples prior to and after extraction due to the low oil content in Type C shale samples.

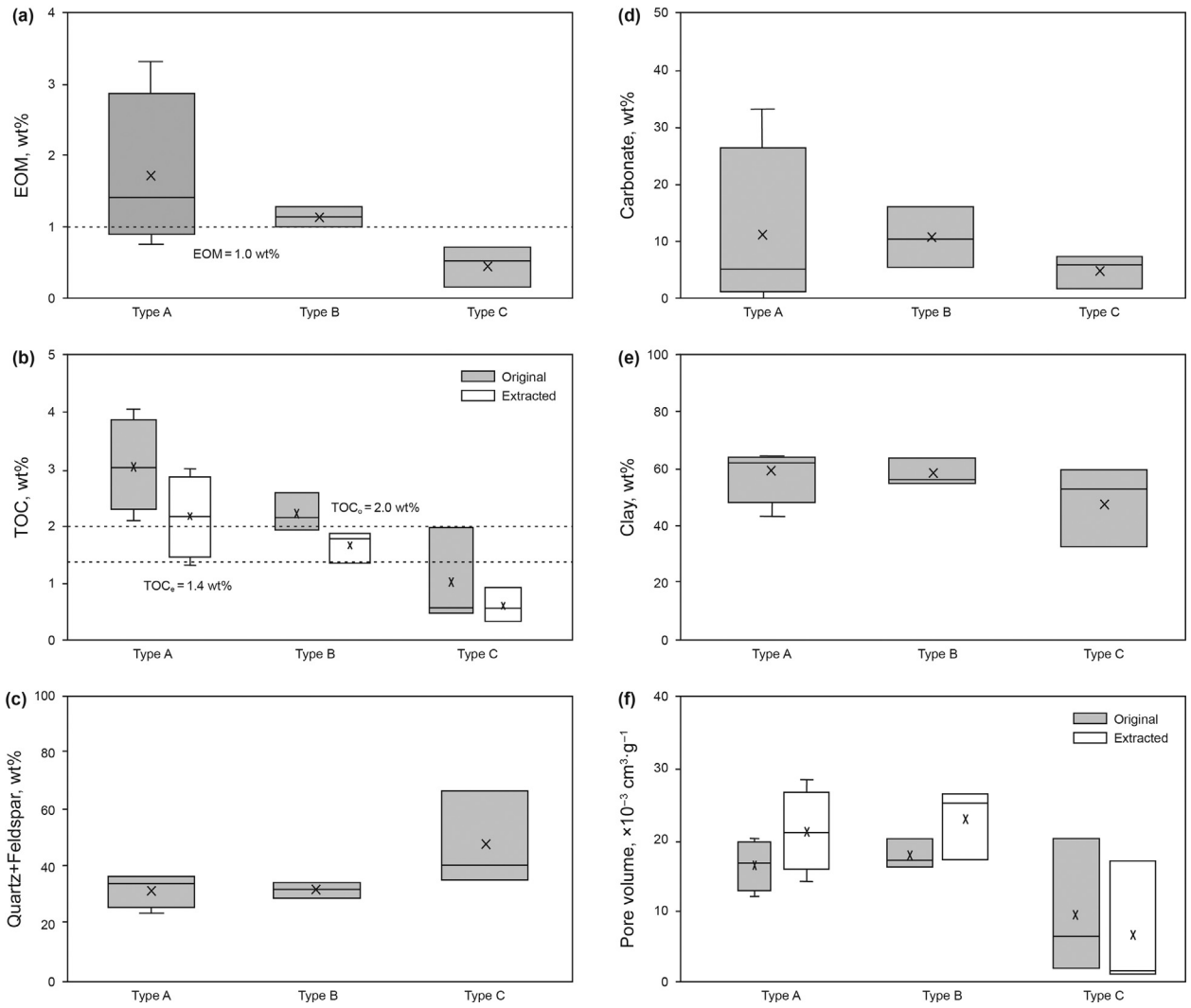

Fig. 7. The minerals and EOM distributions of the shale samples with different nitrogen isotherm types. (a) Content of the EOM. (b) TOC of original and extracted shale samples. (c) Content of the quartz + feldspar. (d) Content of the carbonate minerals. (e) Content of the clay minerals. (f) Pore volume of original and extracted shale samples.

4.3. Mobile oil storage pore space

After extraction, TOC_e has good positive correlations with pore volume and the specific surface area (Fig. 9), indicating that main contribution to the pore volume in the Q1 Formation is mainly the micropores related to OM. Yet, the I2-3 sample is a clear outlier from this correlation. Compared to the other samples, the content of carbonate minerals in the I2-3 sample is relatively high, up to 33.5 wt%. During the oil generation stage, carbonate minerals are easily dissolved forming dissolution pores, which will provide a few of pore volume (Loucks et al. 2015; Dong., 2018). However, the specific surface area does not increase significantly as the dissolution pore developed (Fig. 9a). The correlation between kerogen content and pore volume indicates that OM related pores are well developed in the Q1 Formation, providing a certain space for the accumulation of free oil. At the same time, there is a good negative correlation between pore volume and average pore size (Fig. 5c and d), indicating that the OM pores of the Q1 Formation are mainly nano pores.

The relationship between mobile shale oil distribution and pore size distribution could not be directly examined for any of the samples. However, the differences in pore volume distribution (Δ DV/DW) between unmodified samples and shale samples that have undergone hydrocarbon extraction can directly indicate the distribution of mobile shale oil in pores of different diameters. Hence, in this study, the differences in pore volume distribution from samples prior to and after extraction was used to characterize the distribution in space of mobile shale oil (Fig. 10).

It can be seen that for Type A and B shale samples, shale oil is found in pores with diameters less than 10 nm, followed by pore with diameters of 20 nm and 40 nm. For Type C shale samples, the change in pore diameters is only concentrated at 20 nm and 40 nm, showing a bimodal distribution. Due to the presence of undeveloped pores (diameter <10 nm) and low EOM content, the pore size distribution curves of Type C shale samples prior to and after extraction are not clearly defined, which may be within the error range of nitrogen adsorption experiment. Hence, the Δ DV/DW from Type C shale samples is not always positive (for example, the Δ DV/DW of I1-3 and I2-1 samples are negative), and the pore space after extraction does not increase as expected, but decreases instead. That means that the difference of pore size distribution before and after extraction may not quantitatively reflect the distribution characteristics of mobile oil in pores with different diameters. Examination the differences in pore volume distributions

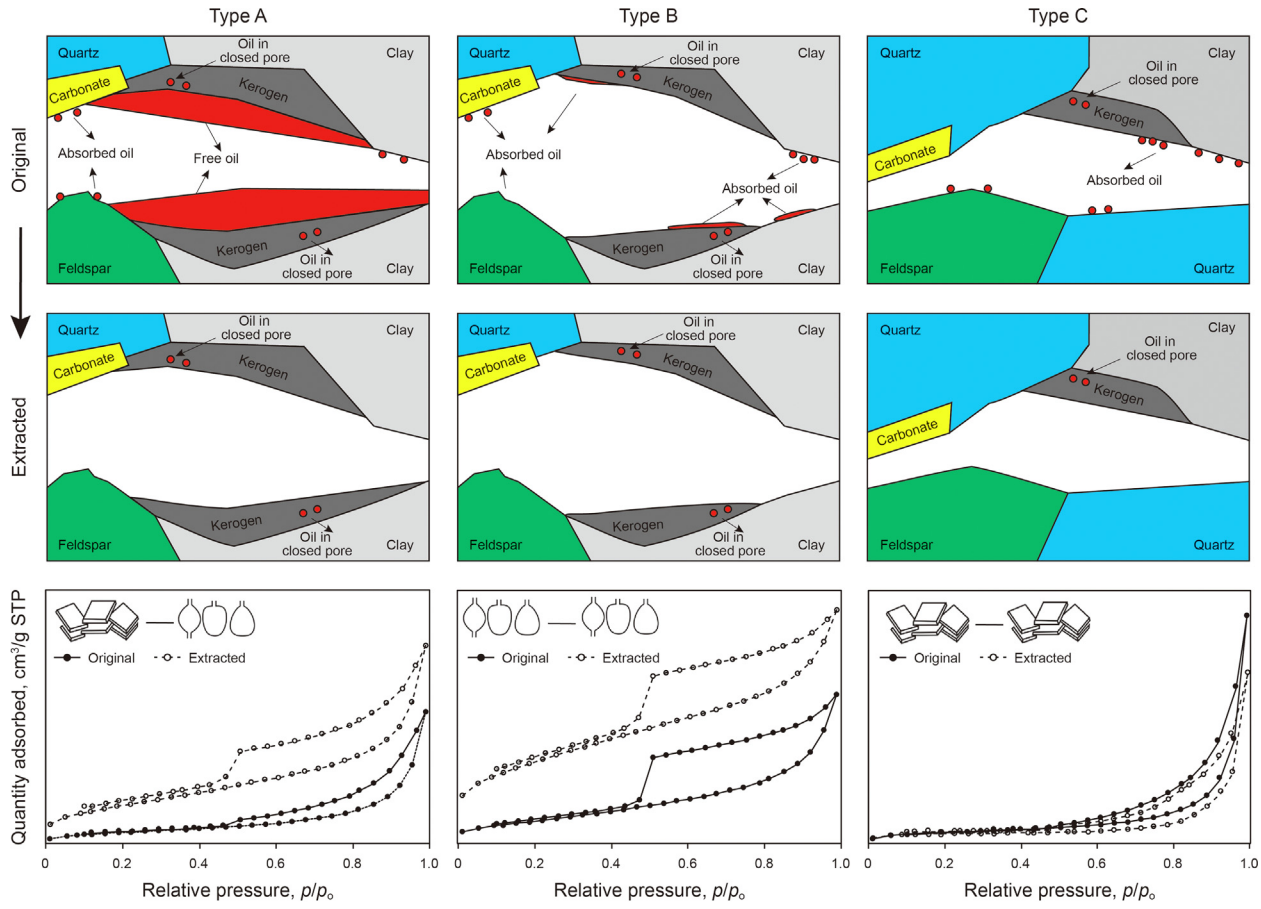

Fig. 8. Schematic illustration of impact of the content of shale oil in different phase states on the nitrogen adsorption isotherms.

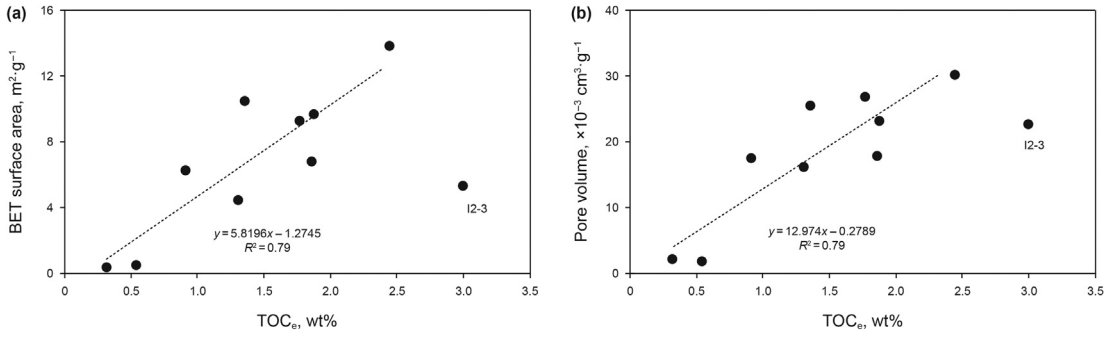

Fig. 9. (a) Crossplots of the TOC versus BET surface area of the extracted shale samples. (b) Crossplots of the TOC versus pore volume of the extracted shale samples.

from samples prior to and following hydrocarbon extraction in Type C shale samples still allows the conclusion to be drawn that shale oil is found in pores with diameters of 10–40 nm.

4.4. Mobile shale oil generation thresholds in the Q1 Formation

Soluble organic matter extraction allows the characterization of most of the stable hydrocarbons in shales, including heavy hydrocarbons. For this reason, EOM is used to quantitatively characterize the content of shale oil in the Q1 Formation. In shale reservoirs, the hydrocarbon content generated could only be discharged on the premise of meeting its own adsorption capacity (Pang et al., 2004; Zhu et al., 2019). In this study, examination of the nitrogen adsorption curves from the Q1 Formation gives an indication of: whether the hydrocarbon content in the samples matches the adsorption capacity of the shale minerals and OM; the phase states of the shale oil; whether the mobile oils were able to migrate into available pore space and change the original pore structure characteristics (Fig. 8). The selected threshold TOC_0 and EOM values for Type A and B shale samples rich in free and adsorbed shale oils and Type C shale samples only containing trace adsorbed shale oil are 2.0 wt% and 1.0 wt% respectively. These values are determined as the oil-bearing threshold values for Q1 shale oil mobility (Fig. 7a and b and Fig. 8). In the 1st stage, the amount of hydrocarbon generation is insufficient to exceed the adsorption capacity of the shale minerals and OM surfaces (EOM <1.0 wt%), and shale oil mainly exists in the adsorption phase state. The values for maximum specific surface area and total pore volume of the shale

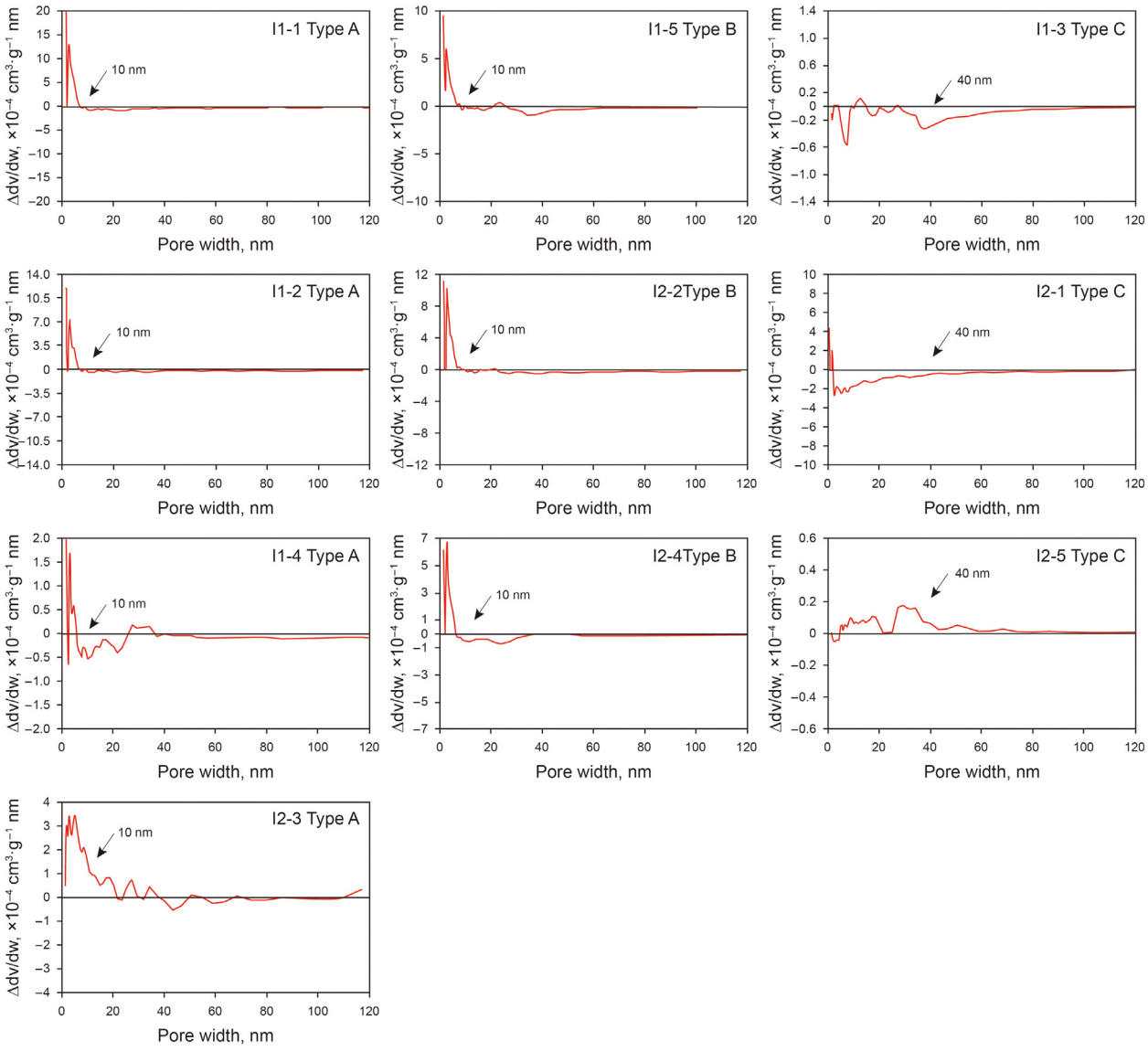

Fig. 10. The pore volume distribution differences between the original and extracted shale samples.

reservoir could reach 6 m^2/g and 20 × 10^{-3} cm^3/g, respectively. In the 2nd stage, the amount of hydrocarbon not only meets the adsorption capacity of shale minerals and OM surface (EOM >1.0 wt %), but also fills the pore space in the shale. The average pore diameter of the extracted shale samples is basically greater than 10 nm (Fig. 5), and the oil extraction process measures the sum total of the produced free and partially adsorbed shale oil at the same time. Besides, within the pore size range of Δ DV/DW less than 10 nm, Type A and B shale samples show a large amount of shale oil occurring in pores with diameters of less than 10 nm (Fig. 10). This is considered to be oil that is in the adsorbed phase state. 10 nm is therefore considered to be the threshold value of pore size that affects the mobility of shale oil in the Q1 Formation.

In the paper by Zhu et al. for shale samples that had undergone hydrocarbon extraction, an EOM value of 0.7 wt% and a minimum average pore diameter of 12.1 nm after extraction were used as the thresholds to determine whether the shale oil content of the samples exceeded the adsorption itself (Zhu et al., 2019). However, in this study there were no samples with TOC less than 1.0 wt%. Therefore, in the 1st stage, when the kerogen content of the sample is low and the hydrocarbon generation does not meet the adsorption of itself, the specific surface area and pore volume of the sample may be affected by other factors such as inorganic mineral composition, resulting in a wide range of EOM and average pore diameter values rather than a single value for each parameter (Fig. 11).

It is worth noting that the thresholds for mobile shale oil defined by this study: average pore diameter (10 nm) and EOM content (1.0 wt%), are based on the study of shale samples from the Q1 Formation. The results on which these thresholds are based are also affected by the quality of crude oil and the development characteristics of the reservoir space, which are different from the shale samples investigated by Zhu et al. (2019) from the Shahejie Formation. The lower pore diameter threshold and the higher content of soluble OM in the Q1 Formation may indicate that the pore space of nanoscale related to OM is better. After the extraction, most of the adsorbed shale oil within pore spaces of less than 10 nm in diameter in Q1 Formation shale is also extracted. Shale oil can be extracted from pores down to around 2 nm in diameter. Previous studies have also shown that the effective molecular diameters of

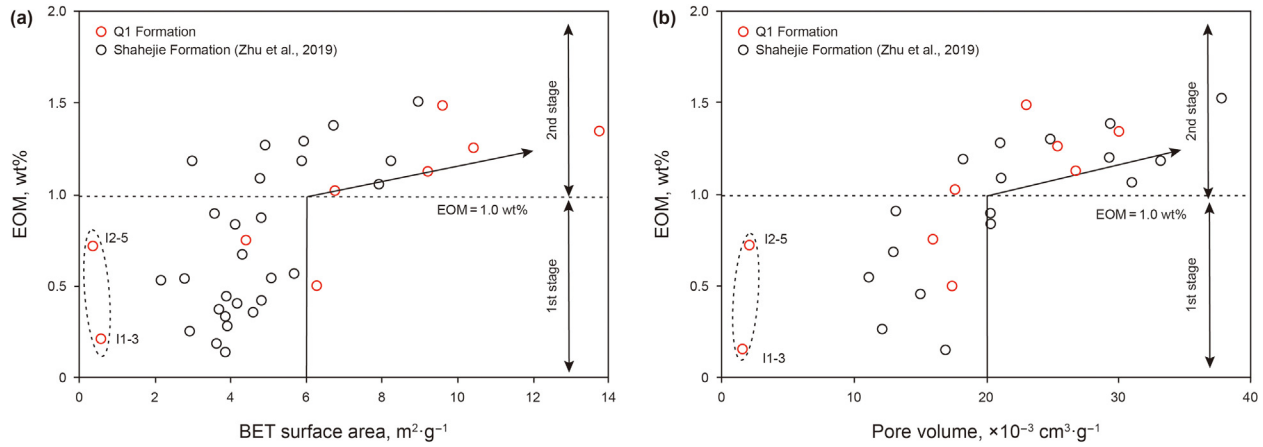

Fig. 11. Crossplots of EOM against BET surface area and pore volume after extraction.

n-alkanes, cyclohexanes, complex ring structures and micro granular compounds are 0.48 nm, 0.54 nm, 1–3 nm and 2–4 nm, respectively (Tissot and Welte., 1984; Wang et al., 1996). Hence, with the improvement of oil exploitation techniques, the pore size threshold for shale oil mobility in the Q1 Formation may fall below 10 nm.

5. Conclusion

1. The nitrogen isotherms of the Q1 Formation shale samples prior to and after extraction can be divided into three types. Type A shales with high kerogen content. Sufficient shale oil fills the pores and oils are primarily in the free phase state. The kerogen content of Type B shales is moderate, and the relatively high shale oil fractional content is mainly in the adsorbed phase state on the surfaces of pore spaces. The kerogen content of Type C shales is relatively low, and the trace amounts of shale oil in these samples is found in the adsorbed phase state on the surfaces of pore spaces. The pore structure in these samples was not affected by oil migration and charge.
2. The content of kerogen controls the content of movable shale oil in the Q1 Formation. The presence of detrital minerals such as quartz and feldspar are conducive to the preservation of pore spaces with diameters of around 40 nm in the Type C samples. The presence of kerogen is conducive to the development of pore space of diameter less than 10 nm in Type A and B samples. Overall, the pore space in the Type C samples is considered to be poorly developed.
3. A large amount of absorbed shale oil contained in the Q1 Formation shale reservoir is found in pores with diameters less than 10 nm. Only when TOC_o is more than 2.0 wt%, the shale oil content (EOM) is greater than 1 wt%, and the average pore diameter is greater than 10 nm, does the shale oil volume exceed the reservoir's adsorption capacity, fill the available pore space and primarily exist in the free phase state.

Acknowledgements

This work was financially supported by the National Natural Science Foundation of China (No.41972156) and the Science and Technology Project of Heilongjiang Province (No.2020ZX05A01).

References

Barrett, E.P., Joyner, L.G., Halenda, P.P., 2014. The determination of pore volume and area distributions in porous substances. I. Computations from nitrogen isotherms. Manag. Eng. 24 (4), 207–216. https://doi.org/10.1021/ja01145a126.
Behar, F., Beaumont, V., Penteado, H., 2001. Rock-eval 6 Technology: performances and developments. Oil & Gas Science and Technology – Rev. IFP. 56 (2), 111–134. https://doi.org/10.2516/ogst:2001013, 2001.
Carvajal-Ortiz, H., Gentzis, T., 2015. Critical considerations when assessing hydrocarbon plays using Rock-Eval pyrolysis and organic petrology data: data quality revisited. Int. J. Coal Geol. 152, 113–122. https://doi.org/10.1016/j.coal.2015.06.001.
Collins, D., Lapierre, S., 2014. Integrating solvent extraction with standard pyrolysis to better quantify thermal maturity and hydrocarbon content in the oil window. URTeC, 1922397. https://doi.org/10.15530/urtec-2014-1922397. Unconventional Resources Technology Conference, Denver, Colorado, USA, 25-27 August.
Curiale, J.A., Curtis, J.B., 2016. Organic geochemical applications to the exploration for source-rock reservoirs - a review. J. Unconv. Oil Gas Resour. 13, 1–31. https://doi.org/10.1016/j.juogr.2015.10.001.
Curtis, M., Brian, J., Carl, H., 2012. Development of organic porosity in the Woodford Shale with increasing thermal maturity. Int. J. Coal Geol. 103, 26–31. https://doi.org/10.1016/j.coal.2012.08.004.
Dong, T., Harris, N.B., Knapp, L.J., et al., 2018. The effect of thermal maturity on geomechanical properties in shale reservoirs: an example from the Upper Devonian Duvernay Formation, Western Canada Sedimentary Basin. Mar. Petrol. Geol. 97, 137–153. https://doi.org/10.1016/j.marpetgeo.2018.07.007.
Dong, T., Harris, N.B., Mcmillan, J.M., et al., 2019. A model for porosity evolution in shale reservoirs: an example from the upper devonian duvernay formation, western Canada sedimentary basin. AAPG (Am. Assoc. Pet. Geol.) Bull. 103 (5), 1017–1044. https://doi.org/10.1306/10261817272.
Espitalié, J., Marquis, F., Barsony, I., 1984. Geochemical logging - ScienceDirect. Analytical Pyrolysis 276–304. https://doi.org/10.1016/B978-0-408-01417-5.50013-5.
Gao, Z., Fan, Y., Xuan, Q., et al., 2020. A review of shale pore structure evolution characteristics with increasing thermal maturities. Advances in Geo-Energy Research 4 (3), 247–259, 0.46690/ager.2020.03.03.
Gao, Z., Hu, Q., 2016. Wettability of Mississippian Barnett Shale samples at different depths: investigations from directional spontaneous imbibition. AAPG (Am. Assoc. Pet. Geol.) Bull. 100 (1), 101–114. https://doi.org/10.1306/09141514095.
Gao, Z., Hu, Q., 2018. Pore structure and spontaneous imbibition characteristics of marine and continental shales in China. AAPG (Am. Assoc. Pet. Geol.) Bull. 102 (10), 1941–1961. https://doi.org/10.1306/03291817297.
Gamero-Diaz, H., Miller, C.K., Lewis, R., 2013. sCore: A Mineralogy Based Classification Scheme for Organic Mudstones. https://doi.org/10.2118/166284-MS.
Ghanizadeh, A., Amann-Hildenbrand, A., Gasparik, M., et al., 2014. Experimental study of fluid transport processes in the matrix system of the European organic-rich shales: II. Posidonia Shale (Lower Toarcian, northern Germany). Int. J. Coal Geol. 123, 20–33. https://doi.org/10.1016/j.marpetgeo.2013.10.013.
Gong, L., Wang, J., Gao, S., et al., 2021. Characterization, controlling factors and evolution of fracture effectiveness in shale oil reservoirs. J. Petrol. Sci. Eng. 203, 108655. https://doi.org/10.1016/j.petrol.2021.108655.
Hu, Q., Zhang, Y., Meng, X., et al., 2017. Characterization of micro-nano pore networks in shale oil reservoirs of paleogene Shahejie Formation in dongying sag of bohai bay basin, east China. Pet. Explor. Develop. 44 (5), 720–730. https://doi.org/10.1016/S1876-3804(17)30083-6.
Huang, Z., Chen, J., Xue, H., et al., 2013. Microstructural characteristics of the cretaceous Qingshankou formation shale, Songliao Basin. Petrol. Explor. Dev. 40 (1), 58–65. https://doi.org/10.1016/S1876-3804(13)60006-3.
Jarvie, D.M., 2012. Shale resource systems for oil and gas: Part 2- Shale-oil resource systems. In: Breyer, J.A. (Ed.), Shale Reservoirs-Giant Resources for the 21st Century, vol. 97. AAPG Memoir, pp. 89–119. https://doi.org/10.1306/13321447M973489.
Jarvie, D.M., Hill, R.J., Ruble, T.E., et al., 2007. Unconventional shale-gas systems: the

Mississippian Barnett shale of north-central Texas as one model for thermogenic shale-gas assessment. AAPG (Am. Assoc. Pet. Geol.) Bull. 91 (4), 475–549. https://doi.org/10.1306/12190606068.
Kennedy, M.J., Löhr, S.C., Fraser, S.A., et al., 2014. Direct evidence for organic carbon preservation as clay-organic nanocomposites in a Devonian black shale; from deposition to diagenesis. Earth Planet Sci. Lett. 388 (18), 59–70. https://doi.org/10.1016/j.epsl.2013.11.044.
Littke, R., Klussmann, U., Krooss, B., et al., 1991. Quantification of loss of calcite, pyrite, and organic matter due to weathering of Toarcian black shales and effects on kerogen and bitumen characteristics. Geochem. Cosmochim. Acta 55 (11), 3369–3378. https://doi.org/10.1016/0016-7037(91)90494-.
Liu, C., Wang, Z., Guo, Z., et al., 2017. Enrichment and distribution of shale oil in the cretaceous Qingshankou Formation, Songliao basin, northeast China. Mar. Petrol. Geol. 86, 751–770. https://doi.org/10.1016/j.marpetgeo.2017.06.034.
Liu, B., Bai, L., Chi, Y., et al., 2019b. Geochemical characterization and quantitative evaluation of shale oil reservoir by two-dimensional nuclear magnetic resonance and quantitative grain fluorescence on extract: a case study from the Qingshankou Formation in Southern Songliao Basin, northeast. Mar. Petrol. Geol. 109, 561–573. https://doi.org/10.1016/j.marpetgeo.2019.06.046.
Liu, B., He, S., Meng, L., et al., 2021b. Sealing mechanisms in volcanic faulted reservoirs in xujiaweizi extension, northern Songliao basin, northeastern China. AAPG (Am. Assoc. Pet. Geol.) Bull. 105 (8). https://doi.org/10.1306/03122119048.
Liu, B., Shi, J., Fu, X., et al., 2018. Petrological characteristics and shale oil prospection in the lacustrine detrital fine-grained sedimentary system: a case study of the organic rich shales within the first member of Qingshankou Form Pet. Explor. Dev. 45, 884–894. https://doi.org/10.11698/PED.2018.05.08.
Liu, B., Sun, J., Zhang, Y., et al., 2021a. Reservoir space and enrichment model of shale oil in the first member of Cretaceous Qingshankou Formation in the Changling sag, southern Songliao Basin, NE China. Petrol. Explor. Dev. 48 (3), 608–624. https://doi.org/10.1016/S1876-3804(21)60049-6 (in Chinese with English abstract).
Liu, B., Wang, H., Fu, X., et al., 2019a. Lithofacies and depositional setting of a highly prospective lacustrine shale oil succession from the upper cretaceous Qingshankou Formation in the Gulong sag, northern Songliao basin, northeast China. AAPG (Am. Assoc. Pet. Geol.) Bull. 103, 405–432. https://doi.org/10.1306/08031817416.
Liu, K., Ostadhassan, M., 2019. The impact of pore size distribution data presentation format on pore structure interpretation of shales. Advances in Geo-Energy Research 3 (2), 187–197. https://doi.org/10.26804/ager.2019.02.08.
Loucks, R.G., Reed, R.M., Ruppel, S.C., 2012. Spectrum of pore types and networks in mudrocks and a descriptive classification for matrix-related mudrock pores. AAPG (Am. Assoc. Pet. Geol.) Bull. 96 (6), 1071–1098. https://doi.org/10.1306/08171111061.
Pang, X., Sumei, L.I., Jin, Z., et al., 2004. Quantitative assessment of hydrocarbon expulsion of petroleum systems in the niuzhuang sag, bohai bay basin, east China. Acta Geol. Sin. 78 (3), 615–625. https://doi.org/10.1111/j.1755-6724.2004.tb00174.x.
Pepper, A.S., Corvi, P., 1995. Simple kinetic models of petroleum formation: Part1: oil and gas generation from kerogen. Mar. Petrol. Geol. 12 (3), 291–319. https://doi.org/10.1016/0264-8172(95)98381-E.
Pitman, J.K., Price, L.C., Le Fever, J.A., 2001. Diagenesis and fracture development in the bakken formation, williston basin: implications for reservoir quality in the middle member. U.S. Geological Survey Professional 1653, 19. https://doi.org/10.3133/pp1653.
Ross, D.J.K., Bustin, R.M., 2007. Shale gas potential of the lower jurassic gordondalemember, northeastern British columbia, Canada. Bull. Can. Petrol. Geol. l55, 51–75. https://doi.org/10.2113/gscpgbull.55.1.51.
Sing, S., 1985. Reporting physisorption data for gas/solid systems with special reference to the determination of surface area and porosity (Recommendations 1984). Pure Appl. Chem. 57 (4), 603–619. https://doi.org/10.1351/pac198557040603.
Sing, S., Neimark, V., Kaneko, et al., 2016. Physisorption of gases, with special reference to the evaluation of surface area and pore size distribution (IUPAC Technical Report). Pure Appl. Chem. 38 (1). https://doi.org/10.1515/ci-2016-0119.
Slatt, R.M., O'Brien, N.R., 2011. Pore types in the Barnett and Woodford gas shales: contribution to understanding gas storage and migration pathways in fine-grained rocks. AAPG (Am. Assoc. Pet. Geol.) Bull. 95 (12), 2017–2030. https://doi.org/10.1306/03301110145.
Su, S., Jiang, Z., Shan, X., et al., 2018. The effects of shale pore structure and mineral components on shale oil accumulation in the Zhanhua Sag, Jiyang Depression, Bohai Bay Basin, China. J. Petrol. Sci. Eng. 165, 365–374. https://doi.org/10.1016/j.petrol.2018.02.030.
Tissot, B.P., Welte, D.H., 1984. Petroleum Formation and Occurrence, vol. 669. Springer-Verlag. https://doi.org/10.1007/978-3-642-87813-8.
Villarroel-Rocha, J., Barrera, D., Sapag, K., 2014. Introducing a self-consistent test and the corresponding modification in the Barrett, Joyner and Halenda method for pore-size determination. Microporous Mesoporous Mater. 200, 68–78. https://doi.org/10.1016/j.micromeso.2014.08.017.
Wang, X.Y., Song, Y.T., Wang, X.J., 1996. Petroleum Generation and Expulsion Physical Simulation: Method, Mechanism and Application. China University of Petroleum Press, Dongying, China, p. 160.
Xie, X., Amann-Hildenbrand, A., Littke, R., et al., 2019. The influence of partial hydrocarbon saturation on porosity and permeability in a palaeogene lacustrine shale-hosted oil system of the Bohai Bay Basin, Eastern China. Int. J. Coal Geol. 207, 26–38. https://doi.org/10.1016/j.coal.2019.03.010.
Zeng, F., Dong, C., Lin, C., et al., 2021. Analyzing the effects of multi-scale pore systems on reservoir properties-A case study on xihu depression, east China sea shelf basin, China. J. Petrol. Sci. Eng. 203, 108609. https://doi.org/10.1016/j.petrol.2021.108609.
Zhang, L., Xiong, Y., Li, Y., et al., 2017. DFT modeling of CO2 and Ar low-pressure adsorption for accurate nanopore structure characterization in organic-rich shales. Fuel 204, 1–11. https://doi.org/10.1016/j.fuel.2017.05.046.
Zhu, X., Cai, J., Liu, Q., et al., 2019. Thresholds of petroleum content and pore diameter for petroleum mobility in shale. AAPG (Am. Assoc. Pet. Geol.) Bull. 103 (3), 605–617. https://doi.org/10.1306/0816181617517009.
Zou, C., Dong, D., Wang, Y., et al., 2015. Shale gas in China: characteristics, challenges and prospects l (in Chinese with English abstract). Petrol. Explor. Dev. 42 (6), 689–701. https://doi.org/10.1016/S1876-3804(15)30072-0.